nature communications

Article

https://doi.org/10.1038/s41467-024-55026-y

The dynamic triage interplay of Hsp90 with its chaperone cycle and client binding

Received: 23 July 2024

Accepted: 28 November 2024

Published online: 11 December 2024

Check for updates

Xiaozhan Qu[1,2], Simin Wang[1], Shuo Zhao[1], Chanjuan Wan[1], Weiya Xu[1] ✉ & Chengdong Huang[1] ✉

Hsp90, a crucial molecular chaperone, regulates diverse client proteins, impacting both normal biology and disease. Central to its function is its conformational plasticity, driven by ATPase activity and client interactions. However, comprehensive insights into Hsp90's dynamic molecular transitions remain elusive. Using solution NMR spectroscopy, we reveal how ATP binding, hydrolysis, and client engagement drive conformational and dynamic shifts in *E. coli* Hsp90, HtpG, through its chaperone cycle. Pronounced conformational fluctuations occur, especially in regions crucial for nucleotide binding and conformational transitions. ATP binding induces slow-exchanging conformations, representing discrete on-path transition states from open to closed forms, while ATP hydrolysis shifts HtpG into a compact conformation. Client binding acts as an allosteric switch, dynamically priming HtpG for elevated chaperone activity and, therefore, its efficient remodeling. Here, we provide atomic-level insights into Hsp90's functional mechanism, highlighting the interplay of conformation, dynamics, nucleotide, and client interactions.

The heat shock protein 90 (Hsp90), a highly abundant and evolutionary conserved molecular chaperone, plays a crucial role in facilitating the maturation and activation of a diverse array of structurally and functionally distinct client proteins[1–4]. Its broad influence is underscored by its regulation of approximately 10% of the eukaryotic proteome, including critical components such as 60% of the human kinome, 30% of E3 ligases, and 7% of transcription factors[3], positioning it as a central hub of protein homeostasis. Many of these client proteins are essential for signal transduction, establishing Hsp90 as a prime target for anticancer strategies[5–7].

Operating as an ATP-dependent homodimer, Hsp90 comprises three highly conserved domains in each protomer: the N-terminal domain (NTD), responsible for nucleotide binding; the middle domain (MD), primarily involved in client binding; and the C-terminal domain (CTD), mediating dimerization. Structurally, Hsp90s belong to the GHKL (gyrase, Hsp90, histidine kinase, MutL) family of ATPases, classified as a split ATPase with residues essential for ATP hydrolysis located in the MD, including a conserved arginine residue that interacts with the γ-phosphate of ATP.

Previous structural studies of Hsp90s in different nucleotide states have captured a series of snapshots during the ATPase-driven chaperone cycle, suggesting dramatic conformational changes. In the nucleotide-free state, the Hsp90 dimer exhibits a highly dynamic V-shaped conformation, encompassing a wide range of open extended states. Upon ATP binding, substantial structural rearrangements occur in the NTD, including the closure of a crucial structural element known as the 'lid'. This closure facilitates the trapping of bound ATP while exposing a hydrophobic surface that promotes N-terminal dimerization and the swapping of the N-terminal β-strands between interacting NTDs. These local conformational transitions further trigger a domain-level rotation of the NTD, the association between the NTD and MD crucial for ATP hydrolysis, and arm-arm proximity. At this stage, Hsp90 adopts an interdigitated closed arrangement[8]. Subsequent ATP hydrolysis and nucleotide release lead to the chaperone's return to its

[1]MOE Key Laboratory for Cellular Dynamics, Center for Advanced Interdisciplinary Science and Biomedicine of IHM, Hefei National Laboratory for Physical Sciences at the Microscale, Biomedical Sciences and Health Laboratory of Anhui Province, Division of Life Sciences and Medicine, University of Science and Technology of China, Hefei, P.R. China. [2]Zhengzhou Tobacco Research Institute of CNTC, Zhengzhou 450001, China. ✉e-mail: xuweiya@ustc.edu.cn; huangcd@ustc.edu.cn

open conformation[9,10]. Cycling through this well-defined sequence of events, Hsp90 physically associates with its clients and eventually release them in a matured conformation[11–13].

While the described simplified schema derived from studies across different Hsp90 isoforms provides foundational insights into Hsp90's functional machinery[14], it also underscores the limitations of drawing broad conclusions from such fragmented data. Investigations across various species reveal significant variations, particularly concerning the specific conformations of Hsp90 in its ATP-bound and ADP-bound states. These findings underline the marked species-dependent differences and the potential confusion arising from attempts to integrate these diverse results into a unified framework. For instance, studies on the endoplasmic reticulum-resident Hsp90 (Grp94) and yeast Hsp90 have shown divergent results, with ADP-bound configurations ranging from a "twisted V" conformation[15] to a blend of open and more compact structures[10,16]. Furthermore, fluorescence resonance energy transfer (FRET) studies indicate a predominantly open conformation for the ADP-bound yeast Hsp90[17,18], whereas even the two yeast Hsp90 isoforms, the constitutively expressed Hsc82 and the stress-inducible Hsp82, exhibit distinct chaperone cycles[19]. Although some consensus exists that ATP-bound Hsp90 typically adopts a closed conformation[8,14], other studies have identified a spectrum of conformations across different Hsp90 species[10,20,21]. This complexity underscores the necessity for systematic and detailed studies of individual Hsp90 species to truly understand their mechanisms and evolutionary adaptations.

Among Hsp90 isoforms, the *E. coli* Hsp90, known as HtpG, represents the simplest system, lacking co-chaperones and featuring shorter linkers between the NTD and MD (Fig. 1a), thus providing a model for studying Hsp90 machinery. Despite its simplicity, unresolved questions about HtpG's function and dynamics persist (Fig. 1b). Structural studies reveal conflicting data: crystallography suggests a parallel-like configuration for ADP-bound HtpG, while techniques like electron microscopy (EM) and small-angle X-ray scattering (SAXS) show a range of open to more compact structures[9,10,16,21]. The ATP-bound state of HtpG remains particularly elusive, displaying a spectrum from open to closed conformations, contrasting with the consistently closed conformation of its mitochondrial and ER-resident

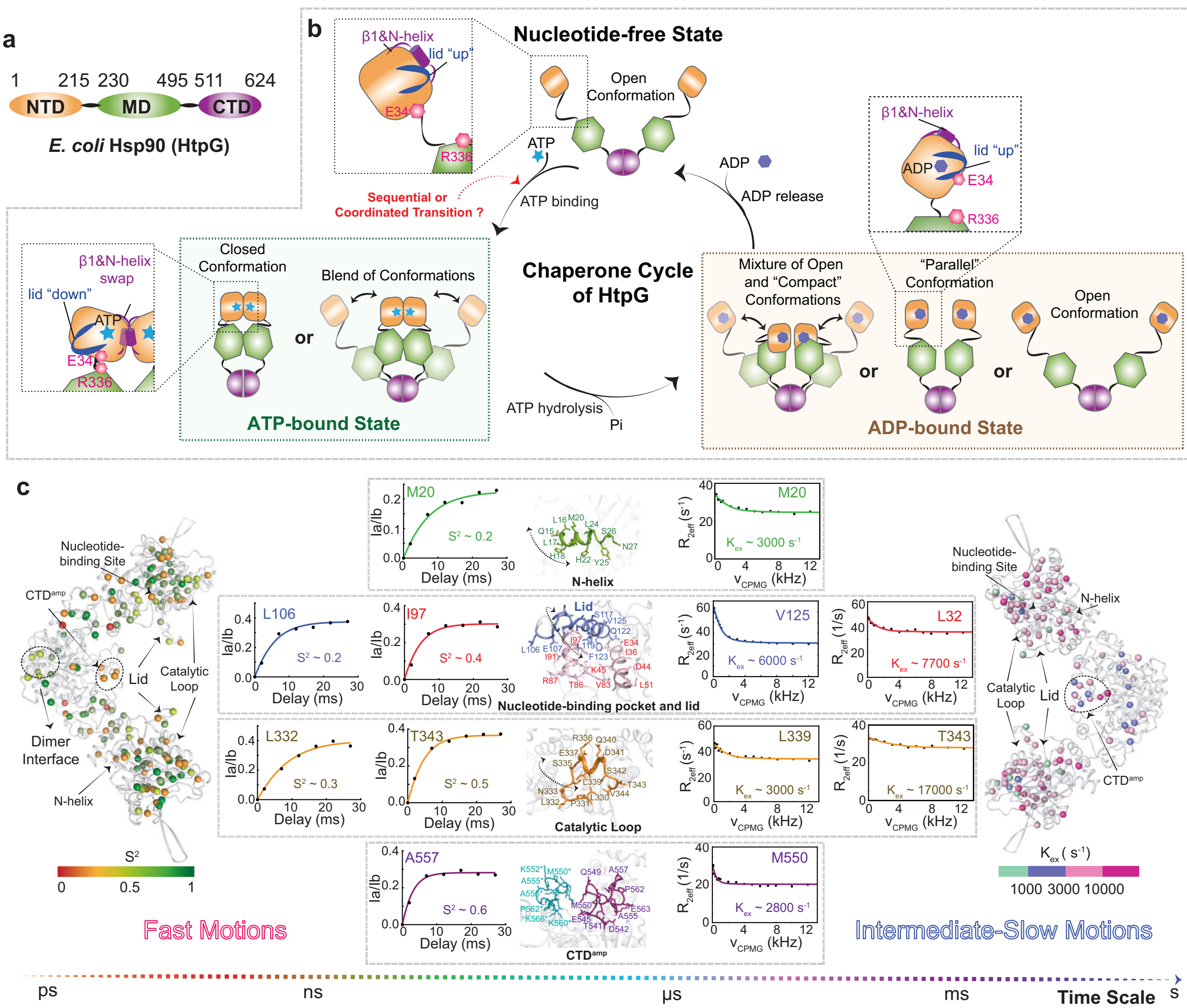

Fig. 1 | Dynamic view of nucleotide-free HtpG. a Domain organization of HtpG, illustrating the three principal domains: N-terminal domain (NTD), middle domain (MD), and C-terminal domain (CTD). **b** Schematic of the conformational transitions of HtpG throughout the chaperone cycle, highlighting various states and existing controversies. **c** Analysis of nucleotide-free HtpG dynamics across different timescales based on its structural context (PDB 2IOQ). The left panel shows methyl groups in HtpG colored according to their S^2 values, representing rigidity, while the right panel colors methyl groups by their microsecond to millisecond timescale exchange rates (k_{ex}). Dashed boxes emphasize detailed profiles of representative residues crucial to HtpG function, accompanied by zoomed-in structural views. More detailed views of the dynamics of nucleotide-free HtpG are presented in Fig. S1.

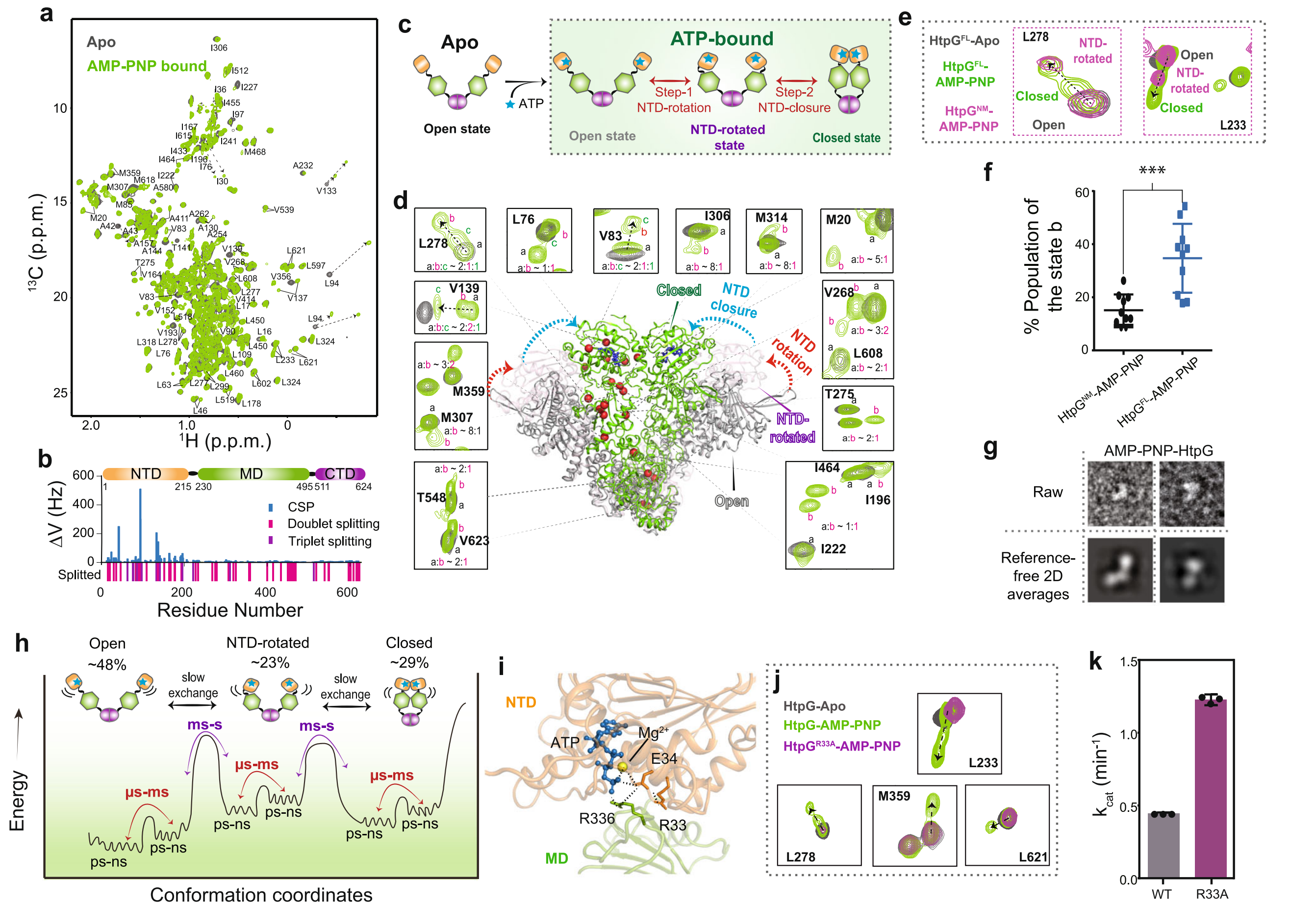

Fig. 2 | Sequential conformational transitions of HtpG induced by ATP binding. **a** Overlay of Methyl-TROSY spectra of apo (gray) and AMP-PNP-bound (green) HtpG, highlighting labeled residues exhibiting resonance splitting. **b** Plot of chemical shift perturbations (CSPs) across residue numbers for AMP-PNP-bound HtpG, with negative bars indicating doublet and triplet splitting signals (rosy and purple, respectively). **c** Schematic representation of the sequential conformational transition pathway of HtpG from the open to the closed state upon ATP binding. **d** Superposition of HtpG structures in open (gray), NTD-rotated (light pink), and closed (green) states, with splitting profiles for selected residues depicted as red spheres. Dashed arrows indicate linear shifts associated with triplet splitting. **e** Overlay of Methyl-TROSY spectra of apo (gray), AMP-PNP-bound (green) HtpG, and HtpG^{NM} in AMP-PNP-bound state (purple) for residues L278 and L233. **f** Population distribution analysis for the second conformational state in AMP-PNP-bound HtpG^{FL} (blue) and HtpG^{NM} (black). Data are presented as individual data points, with mean ± SEM, based on $n = 10$ biological replicates for each group (ten representative residues selected; refer to Methods for details). Statistical significance was assessed using a two-sided t-test, with $p = 0.0004$ as indicated by asterisks. **g** Negative stain EM analysis of AMP-PNP-bound HtpG, with additional images available in Fig. S4. **h** Scheme of the rugged energy landscape for the polymorphic AMP-PNP-bound HtpG. **i** Structural visualization based on PDB 2CG9, illustrating the role of residue R33 in the active site interaction network. **j** Overlay of Methyl-TROSY spectra for apo (gray), AMP-PNP-bound (green) HtpG, and the AMP-PNP-bound HtpG^{R33A} mutant (purple), showing residues representative of the mutation-induced lack of resonance splitting. **k** Comparative analysis of turnover rates between WT-HtpG and the HtpG^{R33A} mutant. Data from three replicates ($n = 3$) are presented as the mean ± SEM.

paralogs, TRAP1 and Grp94[15,22]. Additionally, the transition mechanism of Hsp90 across its nucleotide-driven cycle and the modulation of ATPase activity[23–27] by client protein engagement are poorly understood, not just for HtpG but across the family[28,29]. These gaps underscore the critical need for comprehensive studies to decipher HtpG's molecular intricacies, thereby illuminating the broader regulatory and functional dynamics of the Hsp90 family.

Nuclear magnetic resonance (NMR) spectroscopy stands out as the technique capable of providing atomic-resolution structural and dynamic insights into biological molecules within an aqueous solution, closely resembling physiological environments. Recent advancements in NMR, combined with sophisticated isotope labeling strategies, have extended its applicability to large protein systems[30–37], offering an ideal approach to capture the conformational flexibility and dynamics that characterize the Hsp90 family.

In this work, we use NMR spectroscopy with advanced isotope labeling to investigate the conformational dynamic of HtpG throughout its chaperone cycle. Our findings elucidate the intricate conformational changes and dynamic transitions of HtpG across various nucleotide states, driven notably by ATP binding and hydrolysis, thus revealing its dynamically polymorphic landscape at the atomic-level. Furthermore, we demonstrate how client binding induces widespread alterations in HtpG dynamics, effectively reducing both dynamic and conformational barriers, thereby facilitating chaperone activation. These results offer further insights into the dynamic machinery of Hsp90, illuminating its sophisticated conformational transition and dynamic priming essential for chaperone function.

Results

The dynamic view of HtpG in its nucleotide-free, open state

We have recently achieved NMR assignment of the full-length HtpG and established that the dimeric chaperone in solution adopts an open conformation in the absence of nucleotide, with a single set of NMR signals[38]. To explore the dynamic properties of HtpG in its nucleotide-free state, we first investigated its fast-exchange (pico- to nanosecond, ps-ns) side-chain dynamics using the triple-quantum based NMR experiments[39], and obtained the relaxation-derived order parameter S^2, which quantifies the amplitude of motion ($S^2 = 0$: no restriction; $S^2 = 1$: complete restriction). To ensure accurate interpretation, we limited our analysis to methyl-bearing residues that are well-separated and exhibit feasible intensities—specifically, 83 residues per protomer in the case of apo HtpG. This approach helps avoid the risk of misinterpretation due to overlapping peaks or those with low intensities.

These data reveal that the mobile residues are clustered at (sub) domain junctions and peripheral regions (Fig. 1c and Fig. S1). Notably, the N-helix (residues 15 to 25 in HtpG), which undergoes critical position shifting for HtpG dimer closure[40], displayed significant structural fluctuations (e.g., M20) (Fig. 1c). Elements critical for ATP catalysis, including the nucleotide-binding site (e.g., I97), the "lid" segment that swings substantially to ensure nucleotide docking (e.g., L106), and the so-called catalytic loop (residues 327-343 in HtpG) comprising the absolutely conserved Arg residue (Arg^{336}) in the middle domain (e.g., L332 and T343), whose significant structure remodeling and subsequent reaching to ATP enable catalysis (Fig. 1c)[41], demonstrate moderate to high mobility in absence of nucleotide (Fig. 1c). The significant dynamics at these regions may contribute to moderating nucleotide affinity by providing an entropic barrier. The amphipathic helix in CTD (CTD^{amp}, residues 543-565), known as the "client discriminator helix"[20], demonstrated somewhat structural rigidity at the ps-ns timescale (e.g., A557). Interestingly, the C-terminal dimer interface showed conformational mobility, suggesting a breathing motion[42].

We next investigated the slow-exchange (micro- to millisecond, μs-ms) timescale dynamics in the full-length HtpG using Carr–Purcell–Meiboom–Gill (CPMG) relaxation dispersion experiments, and measured ^1H-^{13}C multiple-quantum methyl-TROSY dispersion profiles[43]. The presence of multiple interconverting states of a protein result in line broadening of the NMR signal, and this effect can be modulated by applying of a series of 180° radiofrequency (RF) pulses in the CPMG pulse sequence[44]. We observed substantial non-flat relaxation dispersions with effective relaxation rates (R_2^{eff}) exceeding 5 S^{-1} in 60 methyl-bearing residues across the HtpG structure, highlighting its dynamic properties (Fig. 1c). These residues, exhibiting intermediate-to-slow motions, are distributed as 29 in the NTD, 21 in the MD, and 9 in the CTD, with one additional residue at the NTD-MD linker. Structural mapping reveal that these mobile residues are predominantly clustered around the nucleotide-binding pocket, the (sub)domain interfaces, and in the vicinity of the CTD^{amp} (e.g., M550) (Fig. 1c and Fig. S1). In contrast, the core regions of the MD and CTD appear predominantly rigid. Notably, this distribution pattern of mobile residues at the domain interfaces aligns with previous computational studies, which suggest that these regions serve as dynamic hinges, facilitating conformational transitions within Hsp90[45]. Particularly, regions crucial for ATPase catalysis, including the N-helix (e.g., M20), lid segment (e.g., V125), nucleotide binding pocket (e.g., L32), and the catalytic loop (e.g., L339 and T343), exhibited apparent conformational plasticity on the μs-ms timescale (Fig. 1c). All dispersion curves could be fit well to a simple two-site exchange process, whereas in most cases the fast-exchanging rates (k_{ex} > 3000 S^{-1}) preclude accurate estimation of populations of exchanging states or chemical shift differences. Notably, the conformational exchange rates of lid segment, as well as other regions involved in nucleotide binding and catalysis, appear significantly higher than that of the nucleotide association/dissociation, suggesting the nucleotide-binding process is largely thermally driven, as previously proposed[16].

Taken together, these results demonstrate the mobility profile of HtpG over a broad spectrum of time scales. The highly dynamic nature of HtpG may contribute for its remarkable capacity to accommodate structurally diverse client proteins, and facilitate its functional structure reorientation.

ATP binding shifts HtpG's conformational equilibrium

As the functional roles of Hsp90 rely on in its distinct, nucleotide-dependent conformational plasticity, we next assessed the conformation of HtpG across various nucleotide states. First, we acquired NMR spectra of HtpG in the presence of AMP-PNP, a "nonhydrolyzable" ATP analogue that has been shown to exert effects identical to ATP[40]. Remarkably, upon binding to AMP-PNP, a significant number of methyl resonances of HtpG (63 out of the 229 methyl-bearing residues per protomer) displayed signal splitting, accompanied by chemical shift perturbations (CSPs) that are primarily localized in the NTD (Fig. 2a, b and Fig. S2a). This signal splitting cannot be attributed to insufficient AMP-PNP supply, as the residues around the nucleotide-binding site (e.g. L94, V133 and V137) shift completely from their original positions (Fig. 2a). Moreover, the splitting is not a result of ADP contamination; spectral overlays confirm that the split signals do not align with those of the ADP-bound HtpG (Fig. S2b). Notably, such signal splitting does not occur in the isolated NTD of HtpG, which only shows significant CSPs upon AMP-PNP binding (Fig. S1c). This indicates a distinct dynamic response of the full-length protein compared to the isolated domain. We have assigned these methyl groups within the AMP-PNP-bound HtpG, including the well-separated split signals (see Methods for details). Further analysis reveals that resonance splitting of methyl moieties extends throughout the entire HtpG molecule, with signals from 11 residues splitting into triplets (Fig. S2d). Among these, seven residues are located around the nucleotide-binding pocket within the NTD, two (M307 and L233) are at the NTD-MD interface, and one (I512) is within the CTD.

Additional sets of NMR signals often indicate the presence of multiple conformational states undergoing slow exchange (k_{ex} <1000 s^{-1}). The evaluation of NMR signal integration demonstrated that different residues displayed varied splitting profiles concerning the number of split resonances and populations of conformational states (Fig. 2d). These observations ruled out the possibility that the NMR resonance multiplet was caused by an asymmetric configuration for each Hsp90 protomer, which would otherwise exhibit a uniformly distributed population profile. For instance, while the residues of L76, V83, L233 and L278 exhibit characteristic of triplet splitting, the population distribution ratio for the three states along the conformation transition pathway (states a, b and c, respectively) ranges from 5:1:4 to 2:1:1 (Fig. 2d). Residues displaying a doublet splitting profile, such as M20, I222, I306 and T548, exhibited populations ratio of states a and b ranges from 8:1 to 1:1 (Fig. 2d). These results thus provide a multifaceted and highly polymorphic perspective of HtpG in its AMP-PNP-bound state.

In the sequential transition model, Hsp90's conformational change from open to closed involves two principal stages: (1) a ~ 90° rotation of the NTD accompanied by local structural alterations and MD association; and (2) arm-arm approximation (Fig. 2c)[20,25]. Our NMR data of HtpG-AMP-PNP may thus provide an allosteric fingerprint of these essential conformational stages, supporting the sequential model. We propose that ATP-bound HtpG exists in an equilibrium of multiple conformational states, spanning all three on-path transitional states: the open state (state a), the intermediate NTD-rotated state (state b), and the closed state (state c). This is supported by multiple lines of evidence. Firstly, NMR spectra of the AMP-PNP bound NTD of HtpG, which lacks integral NTD-MD hinges necessary for rotation, demonstrate no signal splitting (Fig. S2c). Secondly, NMR spectra of the AMP-PNP-bound $HtpG^{NM}$, capable of NTD-rotation but not arm closure due to lacking the dimerization-pivoting CTD, show that conformation transition halts at state b, the NTD-rotated intermediate state (Fig. 2e and Fig. S3a-d). Additionally, signal splitting in residues I306 and M314, corresponding to residues I350 and I358 in yeast Hsp82, has been shown to reflect the conformational transition to the NTD-rotated phase[20]. The inability of residues to transition beyond state b suggests a distinct chemical environment preserved across

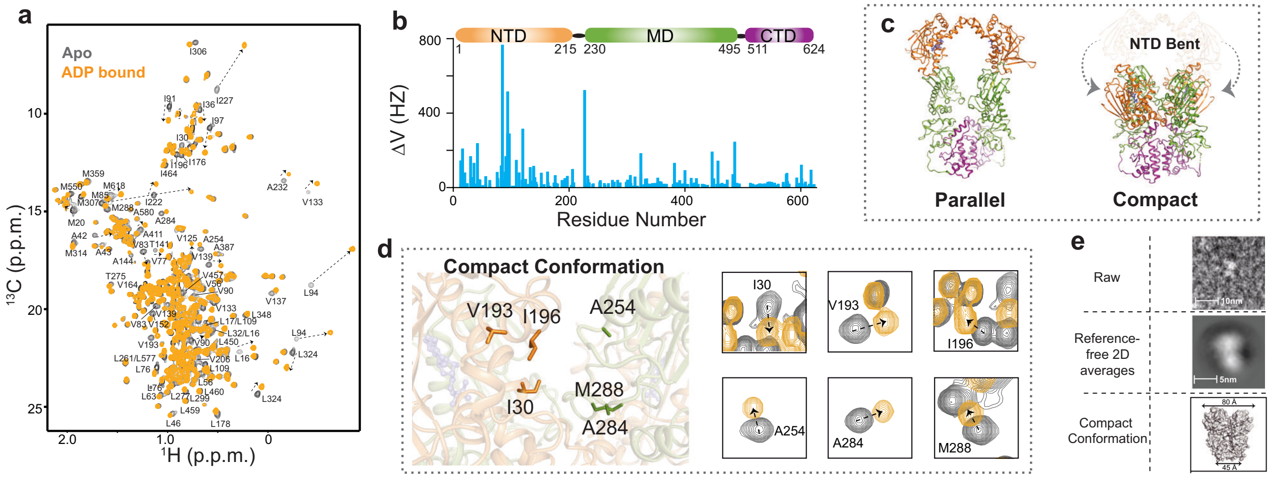

Fig. 3 | ATP Hydrolysis Drives HtpG from Diverse Conformations to a Singular 'Compact' State. a Methyl-TROSY spectra overlay showing apo HtpG (gray) and ADP-bound HtpG (orange), with residues that demonstrate significant shifts labeled. **b** Chemical shift perturbations (CSPs) plotted against residue number for ADP-bound HtpG, illustrating the extent of conformational change upon ADP binding. **c** Structural models of ADP-bound HtpG: on the left, the parallel conformation (PDB 2IOP); on the right, the 'compact' conformation derived from EM data analysis[10]. **d** Detailed view of the 'compact' conformation, highlighting representative residues affected by ADP binding. These CSPs support a significant NTD bending that is incompatible with the parallel conformation. **e** Negative stain EM analysis confirming the 'compact' conformation of ADP-bound HtpG, with additional images available in Fig. S6b,c.

these states, resulting in unchanged chemical shifts or signal degeneration due to rapid averaging. Notably, the arm closure-impaired $HtpG^{NM}$ construct in its AMP-PNP-bound state shows a decreased relative population of state b, aligning with expectations for signal degeneration (Fig. 2f). In the full-length protein, the additional set of peaks represent both the NTD-rotated and closed states, whereas in the $HtpG^{NM}$, they indicate only the rotated state. Lastly, negative stain EM analysis confirms that, in the presence of AMP-PNP, HtpG exhibits both open and closed conformations (Fig. 2g and Fig. S4), consistent with previous SAXS studies[21].

These findings affirm the sequential nature of HtpG's conformational transitions upon ATP binding and highlight the sophisticated regulation of these transitions at the molecular level. Further group analysis of the 11 triplet-splitted residues through signal integration has quantified the populations of the AMP-PNP-bound HtpG conformations: 48 ± 7% in the open state (state a), 23 ± 11% in the intermediate NTD-rotated state (state b), and 29 ± 10% in the closed state (state c). These findings suggest that the conformations of AMP-PNP-bound HtpG are best represented by a rugged energy landscape, as illustrated in Fig. 2h.

HtpG closure is not required for ATP hydrolysis

Prior research has established the conserved arginine residue in the α2 (R33 in HtpG) as a critical conformational switch within the interaction network between the NTD and MD of Hsp90 and ATP[20,46] (Fig. 2i). Supporting the transition scenario mentioned above (Fig. 2c), mutation of R33 impedes the transition from the open to the closed state, as evidenced by the absence of resonance splitting in the NMR spectra of the $HtpG^{R33A}$ mutant bound to AMP-PNP (Fig. 2j and Fig. S3d and S5a,b), which indicates a halt at the open state and an inability to progress along the transition pathway. Furthermore, the R33 mutation induces extensive chemical shift perturbations beyond the NTD, including in MD residues such as I222, I306, and L324, underscoring its central role in the conformational modulation of Hsp90 (Fig. S5a).

The necessity of conformational closure for ATP hydrolysis by Hsp90 has remained uncertain. To address this, we measured the ATPase activity of the conformation-transition impaired mutant, $HtpG^{R33A}$, finding it to exhibit substantial catalytic activity—approximately 80% greater than that of the wild-type protein (Fig. S5c). This mutant, despite its inability to achieve dimer closure, efficiently catalyzes ATP hydrolysis. Further enzymatic kinetics analysis revealed that the mutation leads to an approximately 2.7-fold increase in turnover rates, while the Michaelis-Menten constant (K_m) remains largely unchanged (Fig. 2k and Fig. S5d,e). These findings align with hybrid quantum/classical (QM/MM) free-energy calculations[46], which suggest that mutation of the conserved arginine residue significantly lowers the reaction energy barrier, thereby enhancing the catalysis rate.

ATP Hydrolysis drives HtpG to a 'compact' conformation

We next sought to use NMR to elucidate the conformational state of the ADP-bound HtpG in solution. In sharp contrast to the split spectra observed for AMP-PNP-HtpG, the ADP-bound chaperone displays a singular methyl-TROSY resonance set (Fig. 3a and Fig. S6a), suggesting both HtpG protomers are uniformly sampling the same conformational space within the fast-exchange NMR timescale, specifically under 1 ms, without slow conformation exchanging events occurring. This observation precludes slow conformational exchange events and indicates a homogenous conformation as opposed to a heterogeneous mixture, challenging previous assertions based on negative stain EM and SAXS studies[10]. Furthermore, ADP binding induced substantial chemical shift perturbations (CSPs), mapping not only to the NTD containing the nucleotide pocket, but throughout all three HtpG domains and the inter-domain linkers (Fig. 3b). These widespread CSPs suggest ADP binding triggers global conformational rearrangements in HtpG. The controversy surrounding whether ADP-bound HtpG assumes a parallel[9] or a more 'compact' conformation[10], with the NTD bending toward the MD, persists (Fig. 3c). However, NMR's high conformational sensitivity enabled the distinction between these two disparate structures. Specifically, the 'compact' conformation, characterized by the NTD's extensive interaction with the MD, was evidenced by significant CSPs at the interface, notably at residues I30, V193, I196, A254, A284, and M288 (Fig. 3d). These perturbations are consistent with the 'compact' model and cannot be readily explained by a parallel orientation. Thus, our NMR findings support the conclusion that HtpG predominantly adopts a 'compact' conformation in solution, which is further corroborated by our negative stain EM data (Fig. 3e and Fig. S6b,c).

https://doi.org/10.1038/s41467-024-55026-y

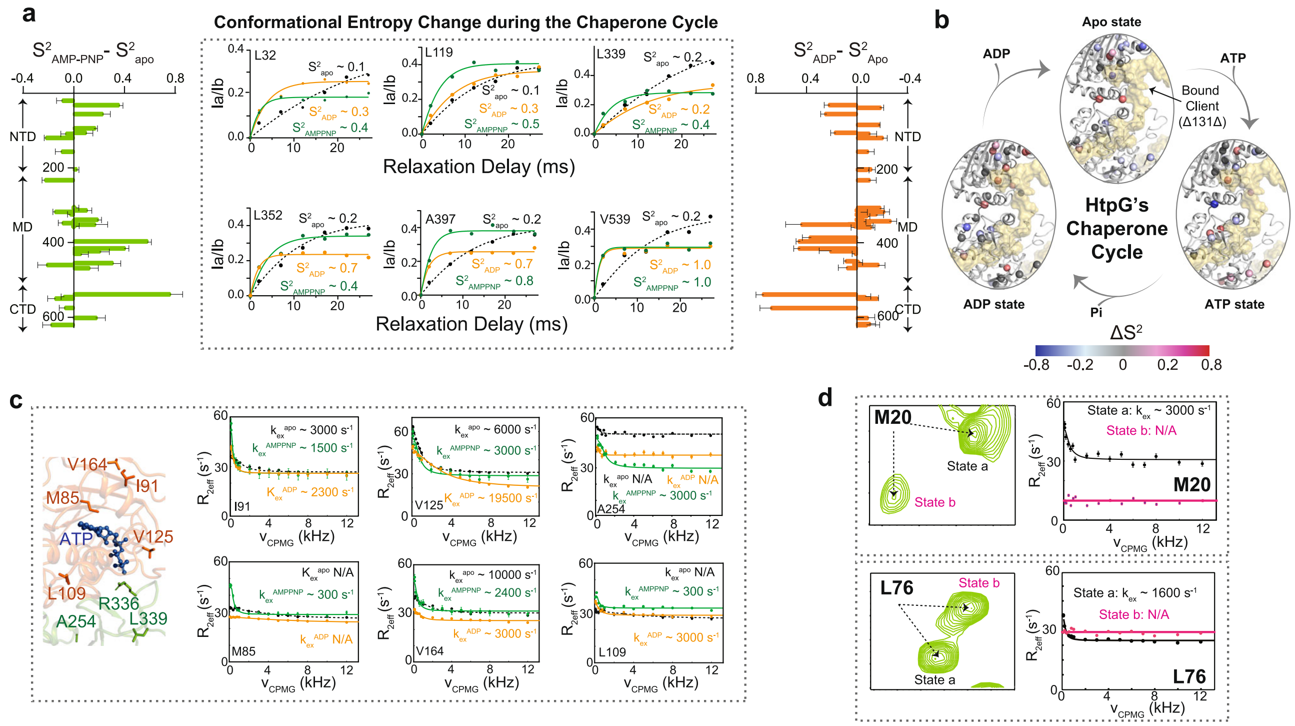

Fig. 4 | Dynamic changes in HtpG across its chaperone cycle. a Global shifts in conformational entropy of HtpG across different nucleotide states. The left panel shows changes in the order parameter (S^2) upon AMP-PNP binding, calculated from single measurements of each protein sample. Data points represent changes for each residue, with error bars indicating propagated standard errors based on uncertainties in the S^2 values derived from spectral data. The right panel displays changes upon ADP binding, with data plotted against residue numbers. The center panel depicts representative S^2 profiles for selected residues across various nucleotide states. **b** Structural representation of ps-ns motion changes of methyl groups near the client-binding grooves, colored by changes in order parameters (ΔS^2). ΔS^2 is calculated as the difference between the current and the previous nucleotide state values. The bound client protein (Δ131Δ) is represented as a transparent yellow surface. The figure was prepared using PDB 8K2T. Fit profiles for selected individual residues are displayed in Fig. S7a. **c** Characteristic relaxation dispersion profiles of active site residues in HtpG across different nucleotide states, accompanied by a structural illustration on the left. This panel highlights the residue-specific dynamics that underpin functional transitions. **d** Conformation-specific CPMG profiles for residues M20 (top) and L76 (bottom) in the AMP-PNP-bound state of HtpG, demonstrating distinct dynamical behaviors within the intermediate to slow time regimes. In panels c and d, error bars for R_{2eff} rate values were calculated as twice the noise level measured in the spectra.

Dynamic transitions of HtpG in the ATPase cycle

To ascertain whether the dynamics of HtpG, in addition to its conformations, are modulated during its chaperone cycle, we further employed NMR to characterize the protein's dynamics in complex with AMP-PNP or ADP. For AMP-PNP-bound HtpG, in most cases, our dynamic analysis primarily centered on the strongest signals, those corresponding to the open conformation (state a). Both nucleotides were found to significantly influence the order parameters (S^2) across the entire HtpG molecule, including critical regions such as the nucleotide binding pocket (e.g., residue L32), the lid segment (e.g., residue L119), NTD-MD interface (e.g., residues L339 and L352), MD inter-subdomain interface (e.g., residue A397), and MD-CTD joint region (e.g., residue V539), with each nucleotide state displaying distinct dynamic signatures (Fig. 4a). This data indicates that nucleotide engagement at the NTD has a far-reaching effect, allosterically modulating HtpG's movements across the ps-ns timescale. In particular, regions proximal to the nucleotide-binding site exhibited decreased mobility, suggesting an entropically favorable environment for nucleotide accommodation (Fig. 4a). Of note, AMP-PNP binding, compared to the apo or ADP-bound state, increases the order parameter for the catalytic loop residue L339 from ~0.2 to 0.4 (Fig. 4a). This change implies that ATP's gamma-phosphate rigidified the catalytic loop "breathing motion," corroborating its role in reinforcing the NTD-MD contacts[47].

We recently elucidated the solution complex structure of HtpG with a disordered client (Δ131Δ)[38]. Here we explored the dynamic transitions in the client-engagement regions during the chaperone cycle. Our results reveal a complex dynamic transition profile, with residues proximal to or within the client-binding grooves displaying stage-specific mobility patterns (Fig. 4b and Fig. S7a). These subtly refined dynamic environments may exert distinct chaperoning influences on the client at each stage of the cycle, potentially facilitating their processing.

CPMG experiments have provided further insights into the μs-ms timescale dynamics of HtpG during the distinct stages of the chaperone cycle. In particular, residues M85, I91, L109, V125, and V164 near the nucleotide pocket and A254 at the NTD-MD interface exhibited individualized relaxation dispersion profiles according to the nucleotide state (Fig. 4c). While AMP-PNP binding appears to stabilize the nucleotide-binding pocket and surrounding residues—evidenced by the decreased conformational exchange rates for residues such as I91, V125, and V164—this is not uniform across all residues (Fig. 4c and Fig. S7b,c). Conversely, the ADP state revealed a varied response, with some residues (e.g., residues L109 and V125) displaying increased exchange rates and others showing decreased (e.g., V164) or unchanged rates (e.g., M85). These differences in the conformational exchange rates of residues around the nucleotide-binding pocket, notably higher in the ADP-bound state compared to AMP-PNP (e.g. I91 and V125), align with the more rapid kinetics of ADP binding and release, shedding light on nucleotide turnover rates. Notably, the μs-ms dynamics of the catalytic loop residue L339 remained largely unchanged (Fig. S7b), exhibiting an exchange rate (k_{ex} ≈ 3000 s^{-1}) that greatly surpasses the catalytic rate (k_{cat}≈0.005 s^{-1}). This suggests that movements of the catalytic loop

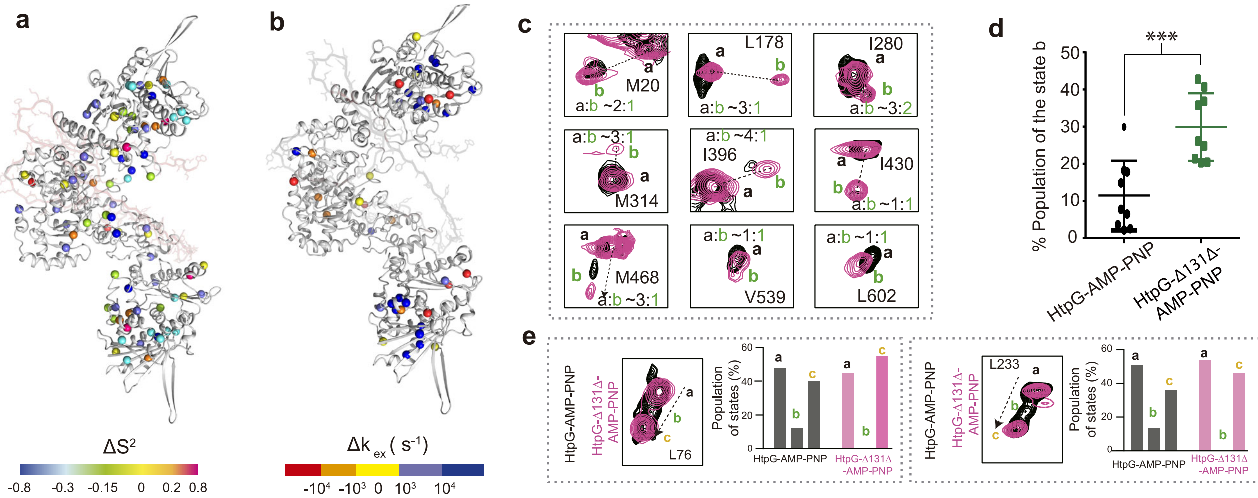

Fig. 5 | Client binding primes the global dynamics and conformational equilibrium of HtpG. a Structural view of ps-ns motion changes of methyl groups upon client binding, colored by the values of changes in order parameters, ΔS^2, which is defined as $\Delta S^2 = S^2_{HtpG\text{-}\Delta131\Delta} - S^2_{HtpG}$. HtpG is shown in gray, with the bound client protein (Δ131Δ) represented in light pink. The figure was prepared using PDB 8K2T. **b** Structural view of μs-ms timescale motion changes of methyl groups colored by the values of changes in exchange rates on the μs-ms time scale Δk_{ex}, which is defined as $\Delta k_{ex} = k_{ex}^{HtpG\text{-}\Delta131\Delta} - k_{ex}^{HtpG}$. **c** Methyl-TROSY spectral overlay for representative residues that exhibit resonance split in unliganded HtpG (black) and HtpG-Δ131Δ (pink), annotated with transition states and population ratios. **d** Population distribution analysis for the second conformational state in AMP-PNP-bound HtpG (gray) and AMP-PNP-bound HtpG-Δ131Δ (green). Data are presented as individual data points with mean ± SEM, based on $n = 9$ biological replicates for each group (nine representative residues selected; refer to Methods for details). Statistical significance was assessed using a two-sided t-test, with $p = 0.0006$ as indicated by asterisks. **e** Population analysis of three split states for L76 (left) and L233 (right) in unliganded HtpG (gray) and HtpG-Δ131Δ (pink), presented as bar graphs.

are not the rate-limiting step for ATP hydrolysis, in agreement with prior observations[47].

In the nucleotide-bound states (AMP-PNP or ADP), specific residues within the client-binding groove, such as M314, L400, A411 and L447, demonstrate reduced dynamics compared to the nucleotide-free state (Fig. S7c). This high flexibility when nucleotide-free may be crucial for initially positioning or accommodating diverse client proteins, thereby preparing the chaperone for subsequent functional stages. Moreover, these dynamic alterations across the chaperone cycle are likely vital for the effective modulation of client protein release and folding processes.

Furthermore, each conformational state of AMP-PNP-bound HtpG, as illustrated by residues M20 and L76, presented distinct CPMG profiles within the intermediate to slow exchange time regime (Fig. 4d). This observation introduces an additional dimension of dynamic intricacy, underscoring the complex conformational landscape that HtpG navigates during its functional cycle.

Collectively, our findings assemble a detailed picture of the dynamic reconfiguration of HtpG throughout its chaperone cycle, presenting the nuanced allosteric regulation and conformational adaptability essential to its function.

The dynamic response of HtpG to client binding

The modulation of Hsp90 ATPase activity by client binding has been proposed as a general mechanism of the action for the chaperone, however, the underlying mechanism remains unclear. To investigate this aspect in terms of protein dynamics, we conducted NMR analyses on the $^{13}CH_3$ methyl moieties of the HtpG-Δ131Δ complex. The quality of the NMR spectra for the HtpG-Δ131Δ complex is suboptimal[38], permitting reliable analysis of only a subset of residues, such as the dynamics of 34 residues at the picosecond to nanosecond timescale. Surprisingly, we observed an overall increase in ps-ns timescale motion ($\Delta S^2 < 0$) in HtpG upon client binding, particularly around the nucleotide-binding pocket in the NTD (Fig. 5a and Fig. S8a). Notably, A114 and A551, situated in the lid and “client discriminator helix”, respectively, gained a large amplitude of structural mobility in response to Δ131Δ binding, with marked decrease in S^2 values of ~0.5 and ~0.9, respectively (Fig. S8a,c). However, the effects of client binding on HtpG’s internal motions are non-uniform; certain residues, like L339 that at the NTD-MD interface, displayed decreased conformational entropy (Fig. S8a,c).

Consistent with these findings, relaxation dispersion experiments indicated that client binding to the MD caused an overall increase in the fluctuation rates of HtpG at the μs-ms timescale, with many of these residues being remotely located in the NTD, indicating a reduced activation energy barrier for conformational transitions at the catalysis center (Fig. 5b and Fig. S8b,d). Additionally, while the “client discriminator helix” (e.g., A555 and M550), along with residue L360, exhibited significant conformation-exchanging profiles in the client-free form, client binding eliminated any alternative conformational states occurring on the μs-ms timescale (the detection limit of the relaxation dispersion experiments is ~0.5%) (Fig. S8d).

Subsequently, we acquired methyl-TROSY NMR spectra of the HtpG-Δ131Δ complex in the presence of AMP-PNP, displaying resonance patterns akin to the client-free state (Fig. S9a,b). These data indicate that in the AMP-PNP state, the HtpG-Δ131Δ complex, resembling client-free HtpG, adopts multiple conformations in equilibrium. Nevertheless, conformational populations of HtpG-Δ131Δ complex in the AMP-PNP state differ significantly from those of client-free Hsp90 (Fig. 5c,d). For instance, residues M20 and M314 exhibited increased populations of state b, corresponding to the transitioned state upon AMP-PNP binding, by 2- and 3-fold, respectively (Fig. 2d and Fig. 5c). Furthermore, residues L76 and L233 displayed a substantial decrease in the intermediate state (state b) due to Δ131Δ binding, shifting the conformation equilibrium towards the closed state (state c) by around 10% and 15%, respectively (Fig. 5e).

Taken together, our results reveal that despite the spatial separation of ATP hydrolysis and client binding sites in the NTD and MD, respectively, these distinct functional processes are dynamically communicated across the full-length HtpG. In this scenario, client binding reconfigures the global internal motions, potentially lowering the rate-limiting conformational barrier and shifting the conformational equilibrium of Hsp90 during the chaperone cycle, in line with recent yeast Hsp90 studies[20].

Discussion

In this study, we unveil the complex interplay within HtpG, the *E. coli* Hsp90, which is orchestrated by its ATPase-driven functional cycle that meticulously integrates conformational shifts with dynamic transitions. Our findings highlight the mechano-chemical coupling between ATP hydrolysis and the extensive structural rearrangements within HtpG. ATP binding initiates HtpG's transition towards a closed state, setting the stage for an equilibrium among the discrete conformations of open, NTD-rotated intermediate, and closed states. Crucially, the observation of all on-path transition states during this conformational shift, coupled with the demonstrative effects of specific truncation and mutations, strongly support a sequential transition mechanism for HtpG (Fig. 2c). Following ATP hydrolysis, this structural heterogeneity is resolved, and our solution NMR spectra suggest that the chaperone transitions into a distinct, singular 'compact' conformation in its ADP-bound state. This sequence of events yields insights into how the energies from nucleotide binding and hydrolysis are elegantly utilized to drive protein conformational changes.

A noteworthy parallel is drawn with eukaryotic Hsp90 through the R33A mutation, which similarly restricts HtpG to an open state, thereby impeding the transition to subsequent conformations along the pathway (Fig. 2i)[20,46]. This similarity suggests a conserved conformational transition mechanism across prokaryotic and eukaryotic Hsp90s, orchestrated by an electrostatic network between the NTD and the catalytic loop within the MD[46,48]. In this scenario, the allosteric signal of ATP binding, initially detected by the nucleotide-binding pocket, is propagated throughout the entire protein, reaching the client-binding regions. Although ATPase-active, this mutation has proven lethal in the yeast *Saccharomyces cerevisiae*[46]. This underscores that the capacity for structural transition, rather than mere ATPase activity, is crucial for Hsp90's ability to mature and regulate client proteins, a finding that aligns with recent studies[49].

Interestingly, this portrayal of *E. coli* Hsp90's conformational change as being unilaterally linked to ATP hydrolysis appears to diverge from that observed in eukaryotic Hsp90s. FRET analyses suggest that for yeast Hsp90, thermal fluctuations rather than ATP binding or hydrolysis predominantly dictate conformational states, exhibiting minimal directionality in this transformation[16,18]. Previous NMR studies using a yeast Hsp90 construct with the NTD-MD linker deleted did not show appreciable resonance splitting upon AMP-PNP binding[50]. Conversely, recent NMR studies demonstrate that ATP binding induces signal splitting in yeast Hsp90 into doublets—representative of the open and NTD-rotated states[20]—a stark contrast to the triplet signals observed in a significant portion of residues in *E. coli* Hsp90, which span all three identified states (Fig. 2a, d and Fig. S2d). ^{19}F NMR analysis reveals that yeast Hsp90 bound to AMP-PNP adopts a range of conformations, with a ratio of 4:6 between open and closed states, suggesting a somewhat larger proportion of the closed state compared to *E. coli* Hsp90 (Fig. 2h). Meanwhile, the ADP-bound protein predominantly adopts an open conformation[51]. Moreover, SAXS data indicate that human Hsp90 does not exhibit significant conformational changes upon ATP binding[31]. This discrepancy raises an intriguing question about the evolutionary advantages conferred by the distinct conformational states and dynamics between these species-specific Hsp90 homologs.

Additionally, we present distinct dynamic signatures for HtpG at each stage of the chaperone cycle, covering timescales from nanoseconds to milliseconds, which are critical for the chaperone's function. Notably, our dynamics data are in remarkable agreement with previous computational studies. For example, the observed stiffening of the H3 region within the NTD (I30–A50) upon AMP-PNP binding aligns with computational models, where it acts as a critical hinge, and its stiffening is pivotal for the signal transmission propagation from the nucleotide-binding pocket to other domains (Fig. 4a)[52]. Moreover, our CPMG measurements corroborate these computational predictions: regions with high betweenness profiles, indicative of rigidity and resistance to conformational changes, showed no significant exchange, affirming the stability of these allosteric pathways[53]. In contrast, areas identified computationally as dynamic hinges, specifically the NTD-MD and MD-CTD interfaces, exhibited notable motions (Fig. 1c), validating their role in facilitating essential conformational transitions within HtpG[45]. These findings highlight a well-balanced interplay between structural stability and flexibility, crucial for HtpG's allosteric regulation and chaperone activity.

Recent NMR studies on human Hsp90α NTD have identified transiently populated states, presumably representing the lid-closed state, within the isolated domain[54]. Our findings extend this observation, demonstrating that such conformational exchanges are not confined to the NTD but also occur across multiple regions of the full-length *E. coli* Hsp90 molecule. While we cannot yet unambiguously assign these transient states, many are situated near the nucleotide-binding pocket or at (sub)domain interfaces, emphasizing the critical role of this structural plasticity in ATP catalysis and subsequent conformational rearrangements. Notably, the conformational exchange rates are remarkably similar across HtpG, human Hsp90α[54], and yeast Hsp90[17], suggesting a comparable level of structural plasticity conserved across different Hsp90 species.

The precise functional role of Hsp90 ATPase activity in its chaperoning machinery continues to be a subject of debate. While it has been suggested to regulate client interactions[55], our recent findings indicate that the engagement of HtpG with the disordered client Δ131Δ is largely nucleotide-independent[38], consistent with interaction studies of Hsp90 with Tau[31] and p53[20]. Building on the structure of the HtpG-Δ131Δ encounter complex, we have proposed that Hsp90 functions as an ATP-driven mechanochemical clamp, where two protomers synergistically capture discrete hydrophobic segments within client proteins[38]. In this study, we extend our model by demonstrating that HtpG not only adopts distinct conformations but also exhibits distinct dynamic signatures across various nucleotide states. Our findings compile a detailed view of how the ATP-driven chaperone cycle intricately fine-tunes HtpG's dynamic properties, shedding light on its functional mechanisms. Specifically, nucleotide accommodation leads to a reduction in fast timescale motions around the binding pocket (Fig. 4a), creating an entropically favorable environment that prevents premature release and ensures a sufficient processing window for client proteins. Furthermore, nucleotide binding significantly stiffens the otherwise flexible domain-domain interfaces and the long helix H3 in the NTD (Fig. 4a). We propose that this rigidification not only stabilizes the domain-domain contacts, promoting a more compact conformation, but also establishes a rigid pathway essential for the propagation of inter-domain allosteric signals[52].

Furthermore, during the chaperone cycle, the S^2 values of the client-binding grooves in HtpG exhibit subtle but meaningful changes (Fig. 4b and Fig. S7c). The S^2 value, a recognized measure of the rigidity or flexibility within a protein's structure, serves as an indicator of conformational entropy which is crucial for mediating interactions between proteins[56]. Thus, alterations in the conformational entropy environment can profoundly influence the local HtpG-client affinities at multiple sites, facilitating the conformational sampling necessary for optimal client processing. Consequently, the dynamic signatures of HtpG at various stages offer diverse platforms for client processing, each adapted to different phases of the chaperone cycle.

These findings have led us to propose a refined model of Hsp90's chaperoning mechanism (Fig. 6). In this model, the conformations of bound clients are synchronized with Hsp90's open-to-closed conformational cycle, and the local dynamic properties of the client-binding grooves significantly influence transient, low-affinity (re) bindings of clients at multiple sites. This refined understanding suggests that ATP's role extends simply providing mechanical forces for macroscopic manipulation of clients, such as stretching and

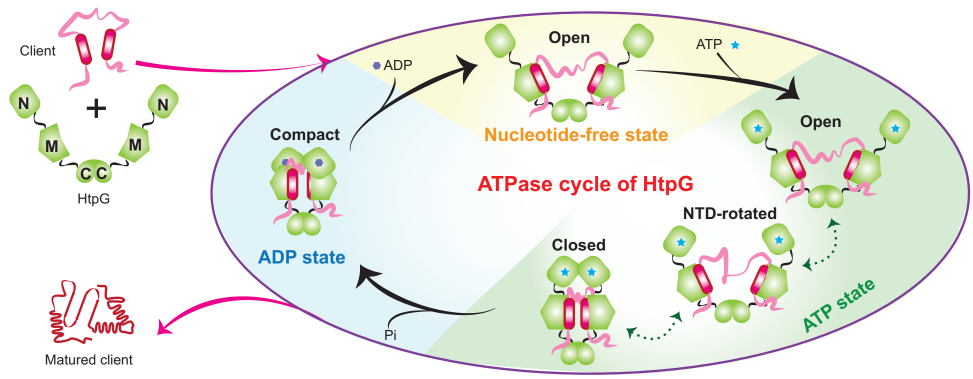

Fig. 6 | Refined model of HtpG's client chaperoning functional cycle. HtpG initially captures the client in its open state, engaging unfolded proteins with one hydrophobic groove on each protomer simultaneously. ATP binding modulates HtpG's conformational equilibrium, promoting a shift towards closure while it remains in a polymorphic state that samples multiple conformations. ATP hydrolysis induces a substantial conformational shift in HtpG, stabilizing it in a distinct, 'compact' state, followed by ADP release which resets the chaperone to its nucleotide-free state. Throughout its cycle, HtpG exhibits distinct dynamic signatures associated with different nucleotide states, illustrated with varying background colors in the figure. This model underscores the dual role of HtpG's ATPase activity in mechanically manipulating clients and precisely regulating molecular dynamics to optimize chaperone function.

squeezing. More subtly, ATP is crucial for fine-tuning the dynamic environments that balance client hold-folding processes at numerous sites, thereby facilitating their conformational sampling and eventual maturation. This comprehensive view highlights ATP's dual function in driving the mechanical aspects of client processing while finely regulating the molecular dynamics essential for optimal chaperone activity.

Our study also presents compelling evidence that client binding instigates a widespread transformation in HtpG dynamics. This transformation effectively triggers chaperone activation by lowering the dynamic and conformational barriers required for the transition to the closed state. These findings enhance our understanding of how client binding intricately regulates Hsp90's ATPase activity. By dynamically adapting to the presence of a client, Hsp90 showcases its capacity to modulate its behavior in response to the cellular context. In this reciprocal interaction scenario, the client binding functions as a dynamic switch, priming Hsp90 with a refined platform that potentially facilitates both the chaperone process and the sampling of client conformations, thereby facilitating efficient client remodeling.

Methods

Expression and preparation of proteins

Protein expression and preparation were carried out using the following constructs: The *E. coli* Hsp90 (residues 1-624), which was cloned into a pET-SUMO vector with an N-terminal 6×His tag and an Ulp1 cleavage site. Additionally, The HtpG^{NM} construct (1-495) was cloned into a pET-16a vector and fused to a 6×His tag, including a tobacco etch virus (TEV) protease cleavage site. Fusion construct between Hsp90 and Δ131Δ was prepared by fusing the Δ131Δ to the C terminus of Hsp90, with a linker of 65 residues to ensure no bias in the complex conformation. The HtpG mutant R33A was generated using PrimeSTAR Max DNA Polymerase (Takara).

All constructs were transformed into BL21(DE3) cells. Cells were grown in LB medium at 37 °C with kanamycin (100 μg/ml). Protein expression was induced by adding 0.1 mM IPTG at OD_{600} ~ 0.5, followed by 4 to 6 hours of incubation at 37 °C.

Purification of proteins

Cells were harvested by centrifugation at 5000 g for 20 min at 4 °C, resuspended in lysis buffer (25 mM Tris-HCl pH 8.0, 500 mM NaCl, 10 mM imidazole, and 1 mM PMSF), and stored at -80 °C until use. After thawing, cells were lysed by a JN-Mini Pro Low-temperature Ultra-high pressure cell disrupter (JNBIO) at 4 °C. The lysate was clarified by centrifugation at 50,000 g for 30 min at 4 °C, and the supernatant was passed through a Ni^{2+}-chelating column (GE Healthcare) pre-equilibrated with lysis buffer.

The column was then washed with 25 mM Tris-HCl pH 8.0, 500 mM NaCl, and 25 mM imidazole to remove non-specifically bound proteins, and the target protein was eluted with 25 mM Tris-HCl pH 8.0, 150 mM NaCl, and 300 mM imidazole. The eluted protein was subjected to TEV protease or SUMO protease cleavage for the removal of amino-end tags by dialysis. Briefly, the eluted protein was mixed with SUMO protease and dialyzed overnight against 50 mM Tris-HCl pH 8.0, 100 mM NaCl, and 1.5 mM β-mercaptoethanol (βme). The protein mixture was then subjected to another round of Ni^{2+}-chelating column purification to subtract the amino-terminal tag and His-tagged TEV protease or His-tagged SUMO protease.

The flow-through was collected, concentrated, and applied to a HiLoad 16/600 Superdex 200 size exclusion column (GE Healthcare). HtpG samples were eluted with 50 mM phosphate pH 7.0, 100 mM NaCl, and 3 mM βme. The purity of each protein was assessed by SDS-PAGE analysis, and the concentration was determined using the Epoch 2 Microplate Spectrophotometer (BioTek) at 280 nm with the corresponding extinction coefficients.

Protein isotope labeling for NMR studies

To produce methyl-protonated samples, we grew cells in 99.9% D_2O (CIL and Isotec) supplemented with D_7, ^{12}C-glucose (2 g/L), [$^{13}CH_3$]-a-ketobutyric acid (46 mg/L), [$^{13}CH_3$]-Met (50 mg/L), [$^2H_2$, $^{13}CH_3$]-Ala (50 mg/L), [$^2H_2$, $^{13}CH_3$]-Thr (50 mg/L), [$^{13}CH_3$]-a-ketoisovaleric acid (85 mg/L), and [$^2H_5$]-Gly (100 mg/L) to the culture 30 minutes before adding IPTG.

NMR spectroscopy

Isotopically labeled samples were prepared in 50 mM phosphate pH 7.0, 100 mM NaCl, 0.05% NaN_3, and 7% D_2O. NMR experiments were conducted using Bruker Avance III 600 MHz and 850 MHz spectrometers that are equipped with cryogenic probes. NMR data were acquired using Topspin 4.0.9. NMR experiments of HtpG and its complex were conducted at 37 °C. The protein sample concentrations ranged from 0.5 to 1.0 mM. Nucleotides were added to a final concentration of 10 mM. All NMR spectra were processed by NMRPipe[57] and analyzed using the NMRViewJ software [http://www.onemoonscientific.com].

NMR assignments of HtpG in various nucleotide states and population analysis of split states

We have previously documented the NMR assignments for the apo state of HtpG[38]. Given the excellent resonance correspondence between the isolated N-terminal domain (NTD) and the full-length (FL) protein across various nucleotide states, we initially assigned the NTD in its AMP-PNP- and ADP-bound states using conventional methods. Sequential backbone and side-chain assignments were accomplished through standard triple-resonance NMR pulse sequences employing nonuniform sampling, including HNCACB, HN(CO)CACB, HNCA, HNCO, HN(CO)CA, HN(CA)CO, and HBHA(CO)NH. Methyl group side-chain assignments utilized three-dimensional (3D) ^{1}H–^{13}C HMQC–NOESY with ^{1}H–^{13}C HMQC, ^{1}H–^{13}C HSQC–NOESY with ^{1}H–^{15}N HSQC, and ^{1}H–^{15}N HSQC–NOESY with ^{1}H–^{13}C HSQC experiments. All NOESY spectra were acquired using the SOFAST version with a mixing time of 300 ms. Typically, each NOESY experiment required 80 scans and spanned an acquisition period of approximately four days. Protein sample concentrations varied from 0.6 to 2.0 mM.

Subsequent to NTD assignments, $HtpG^{NM}$ samples in various nucleotide states were prepared, and data from 3D ^{1}H–^{13}C HMQC–NOESY with ^{1}H–^{13}C HMQC experiments were collected. Spectral overlays confirmed that the majority of assignments from the isolated NTD were transferrable to this construct. Methyl-methyl NOE analysis helped resolve any remaining ambiguities.

Assignments for $HtpG^{NM}$ were then extrapolated to the full-length HtpG, with CTD assignments refined through spectral comparison. Notably, significant CSPs were observed predominantly in the NTD. In contrast, CSPs in MD and CTD were moderate, consistent with structural studies indicating limited conformational changes in these domains during the chaperone cycle.

The assignment of split resonances of the AMP-PNP-bound $HtpG^{NM}$ and $HtpG^{FL}$, indicative of multiple conformational states, presented challenges due to the large size. Initial attempts to correlate split resonances in the AMP-PNP-bound HtpG using EXSY spectra were hampered by insufficient data quality. Well-separated split resonances were straightforward to assign, whereas ambiguities persisted in cases where it was challenging to identify the origin of split resonances. To address these complexities, we applied a combination of spectral comparison, NOE analysis, and peak intensity analysis. For sufficiently intense signals, NOE patterns were compared, as they should theoretically exhibit similarities. We also anticipated that split resonances would demonstrate lower relative intensities, reflecting the distribution of signal across multiple states. Analysis was confined to avoid residues in central regions where signal overlap was prevalent.

This approach enabled the assignment of ~90% and 100% of the backbone and methyl groups, respectively, for $HtpG^{NTD}$ across various nucleotide states. For the full-length protein, we assigned ~90% of methyl groups for ADP-bound HtpG (190 out of 218 residues) and ~70% for AMP-PNP-bound HtpG (Fig. S10a-d).

For the statistical analysis of the population of split states in Figs. 2f and 5c, nine residues (M20, L178, I280, I306, M314, I396, I430, I464, and M468) and ten residues (M20, L76, V133, I222, T275, I306, M314, M359, I433, and I464) were consistently selected across protein samples based on their well-separated peaks in the NMR spectra, ensuring reliable data. Resonance intensity values were extracted using NMRViewJ software. Statistical significance was assessed using a two-sided Student's t-test.

NMR relaxation experiments

To analyze side-chain dynamics in the fast timescale (ps-ns), we used an 850 MHz spectrometer equipped with a Bruker AVANCE III console. We prepared methyl-labeled samples of HtpG, HtpG-AMP-PNP, HtpG-ADP, and HtpG-Δ131Δ fusion in 50 mM phosphate buffer (pH 7.0, 100 mM NaCl, 0.05% NaN_3, and 7% D_2O) and collected relaxation data at 37 °C. The homogeneity of all samples was confirmed by dynamic light scattering, and the global rotational correlation time (τ_c) was determined. Spectra were collected using an interleaved acquisition scheme with relaxation delays of 2, 7, 12, 17, 22, 27, 32, 37, and 42 ms. The order parameters were extracted as described[58].

For changes in order parameter (ΔS^2) values, the propagated standard errors were calculated by combining the individual standard errors of S^2 values from different nucleotide states. The propagated error in ΔS^2 was calculated using the Eq. (1):

$$Error\ in\ \Delta S^2 = \sqrt{\left(Error\ in\ S^2_{state1}\right)^2 + \left(Error\ in\ S^2_{state2}\right)^2} \quad (1)$$

Methyl relaxation dispersion experiments

Multiple-quantum ^{13}C-CPMG experiments were carried out on both 600 and 850 MHz spectrometers equipped with Bruker AVANCE and AVANCE III consoles, respectively. Spectra were acquired in an interleaved manner with CPMG field strength of 100, 200, 300, 400, 500, 700, 1000, 2000, 3000, 4000, 5000, 6000, 8000, 10000, and 12000 Hz on 600 MHz and 100, 200, 400, 600, 800, 1000, 2000, 3000, 4000, 5000, 6000, 7000, 8000, 10000, and 12000 Hz on 850 MHz (Fig. S11a-d). The data were processed using NMRPipe, and peak intensities were extracted using NMRViewJ. Subsequently, the peak intensities were converted to transverse decay rates, R_{2eff}.

k_{ex} and $\varnothing$ were measured by using the Eq. (2)[59]:

$$R_2^{eff} = R_0^2 + \frac{\varnothing}{k_{ex}}\left[1 - \frac{4\upsilon_{CPMG}}{k_{ex}} tanh\left(\frac{k_{ex}}{4\upsilon_{CPMG}}\right)\right] \quad (2)$$

The software NESSY was used to fit the relaxation data[60]. All dispersion curves could be well-fitted to a simple two-site exchange process. However, in most cases, the fast-exchanging rates (k_{ex} > 3000 s^{-1}) hindered accurate estimation of populations of exchanging states or chemical shift differences.

NMR chemical shift perturbations

The interactions of HtpG with nucleotides were monitored by methyl-TROSY experiments. AMP-PNP (10 mM) or ADP (10 mM) was add to 250 μM (dimer concentration) of methyl-labelled Hsp90 in 50 mM phosphate pH7.0, 100 mM NaCl, 0.05% NaN_3, and 7% D_2O. CSPs were calculated in Hz at 850 MHz using the Eq. (3)[61]:

$$\Delta\upsilon = \left(\left(\Delta^1H*850\right)^2 + \left(\Delta^{13}C*213.8\right)^2\right)^{1/2} \quad (3)$$

Negative stain electron microscopy (EM)

For conformation visualization of HtpG at different nucleotide states, we incubated 4 μL of HtpG (0.007 mg/mL) and HtpG (0.007 mg/mL) with AMP-PNP (10 mM) or ADP (10 mM) for 1 h with 20 mM sodium molybdate at room temperature in 25 mM Tris-HCl, pH 8.0, 25 mM KCl, and 10 mM $MgCl_2$. Subsequently, we negatively stained the samples with 1% (w/v) uranyl acetate on carbon-film 400 mesh copper grids and imaged them using a FEI TF20 operated at 200 keV with 62,000× nominal magnification. The structure figures were made using PyMol 3.1 [https://pymol.org/2/].

ATPase activity measurements

Enzymatic assays were carried out according to previously described methods[62]. Briefly, the reactions were performed using 5 μM (monomer concentration) HtpG or $HtpG^{R33A}$ at 37 °C in 25 mM Tris-HCl pH 8.0, 25 mM KCl, 10 mM $MgCl_2$, and 0.5 mM ATP for 1 hour. Steady-state kinetic analysis was performed with 2 μM enzyme under the same conditions, except with various concentrations of ATP from 0.05 to 10 mM. Steady-state kinetic parameters were determined by a double reciprocal Lineweaver-Burk plot for reactions that followed Michaelis-Menten kinetics. The data were analyzed using Prism 10.1.2. All experiments were repeated independently at least three times.

Reporting summary
Further information on research design is available in the Nature Portfolio Reporting Summary linked to this article.

Data availability
The structural data used in this study are available under the following accession codes: 2IOQ, 2IOP, 2CG9, and 8K2T. The NMR assignments of methyl groups for AMP-PNP-bound and ADP-bound $HtpG^{NTD}$ have been deposited in Biological Magnetic Resonance Bank (BMRB) under the accession codes of 52724 and 52725, respectively. The assignments for AMP-PNP-bound and ADP-bound $HtpG^{FL}$ were deposited under the accession codes 52723 and 52722, respectively. The NMR assignment data used in this study are available under the following BMRB accession codes: 52364, 52366, 52720 and 52721. Data supporting the findings of this manuscript are available from the corresponding author upon request. Source data are provided as a Source Data file. Source data are provided with this paper.

References

1. Zhao, R. et al. Navigating the chaperone network: an integrative map of physical and genetic interactions mediated by the hsp90 chaperone. *Cell* **120**, 715–727 (2005).
2. Taipale, M., Jarosz, D. F. & Lindquist, S. HSP90 at the hub of protein homeostasis: emerging mechanistic insights. *Nat. Rev. Mol. Cell Biol.* **11**, 515–528 (2010).
3. Taipale, M. et al. Quantitative analysis of HSP90-client interactions reveals principles of substrate recognition. *Cell* **150**, 987–1001 (2012).
4. Lackie, R. E. et al. The Hsp70/Hsp90 Chaperone Machinery in Neurodegenerative Diseases. *Front Neurosci.* **11**, 254 (2017).
5. Whitesell, L. & Lindquist, S. L. HSP90 and the chaperoning of cancer. *Nat. Rev. Cancer* **5**, 761–772 (2005).
6. Trepel, J., Mollapour, M., Giaccone, G. & Neckers, L. Targeting the dynamic HSP90 complex in cancer. *Nat. Rev. Cancer* **10**, 537–549 (2010).
7. Jaeger, A. M. & Whitesell, L. HSP90: Enabler of Cancer Adaptation. *Annu Rev. Cancer Biol.* **3**, 275–297 (2019).
8. Ali, M. M. et al. Crystal structure of an Hsp90-nucleotide-p23/Sba1 closed chaperone complex. *Nature* **440**, 1013–1017 (2006).
9. Shiau, A. K., Harris, S. F., Southworth, D. R. & Agard, D. A. Structural Analysis of E. coli hsp90 reveals dramatic nucleotide-dependent conformational rearrangements. *Cell* **127**, 329–340 (2006).
10. Southworth, D. R. & Agard, D. A. Species-dependent ensembles of conserved conformational states define the Hsp90 chaperone ATPase cycle. *Mol. Cell* **32**, 631–640 (2008).
11. Verba, K. A. et al. Atomic structure of Hsp90-Cdc37-Cdk4 reveals that Hsp90 traps and stabilizes an unfolded kinase. *Science* **352**, 1542–1547 (2016).
12. Wang, R. Y. et al. Structure of Hsp90-Hsp70-Hop-GR reveals the Hsp90 client-loading mechanism. *Nature* **601**, 460–464 (2022).
13. Noddings, C. M., Wang, R. Y., Johnson, J. L. & Agard, D. A. Structure of Hsp90-p23-GR reveals the Hsp90 client-remodelling mechanism. *Nature* **601**, 465–469 (2022).
14. Schopf, F. H., Biebl, M. M. & Buchner, J. The HSP90 chaperone machinery. *Nat. Rev. Mol. Cell Biol.* **18**, 345–360 (2017).
15. Dollins, D. E., Warren, J. J., Immormino, R. M. & Gewirth, D. T. Structures of GRP94-nucleotide complexes reveal mechanistic differences between the hsp90 chaperones. *Mol. Cell* **28**, 41–56 (2007).
16. Ratzke, C., Berkemeier, F. & Hugel, T. Heat shock protein 90's mechanochemical cycle is dominated by thermal fluctuations. *Proc. Natl. Acad. Sci. USA* **109**, 161–166 (2012).
17. Schulze, A. et al. Cooperation of local motions in the Hsp90 molecular chaperone ATPase mechanism. *Nat. Chem. Biol.* **12**, 628–635 (2016).
18. Mickler, M., Hessling, M., Ratzke, C., Buchner, J. & Hugel, T. The large conformational changes of Hsp90 are only weakly coupled to ATP hydrolysis. *Nat. Struct. Mol. Biol.* **16**, 281–286 (2009).
19. Girstmair, H. et al. The Hsp90 isoforms from S. cerevisiae differ in structure, function and client range. *Nat. Commun.* **10**, 3626 (2019).
20. Lopez, A. et al. Client binding shifts the populations of dynamic Hsp90 conformations through an allosteric network. *Sci. Adv.* **7**, eabl7295 (2021).
21. Krukenberg, K. A., Forster, F., Rice, L. M., Sali, A. & Agard, D. A. Multiple conformations of E. coli Hsp90 in solution: insights into the conformational dynamics of Hsp90. *Structure* **16**, 755–765 (2008).
22. Lavery, L. A. et al. Structural asymmetry in the closed state of mitochondrial Hsp90 (TRAP1) supports a two-step ATP hydrolysis mechanism. *Mol. Cell* **53**, 330–343 (2014).
23. McLaughlin, S. H., Smith, H. W. & Jackson, S. E. Stimulation of the weak ATPase activity of human hsp90 by a client protein. *J. Mol. Biol.* **315**, 787–798 (2002).
24. Motojima-Miyazaki, Y., Yoshida, M. & Motojima, F. Ribosomal protein L2 associates with E. coli HtpG and activates its ATPase activity. *Biochem Biophys. Res Commun.* **400**, 241–245 (2010).
25. Street, T. O. et al. Cross-monomer substrate contacts reposition the Hsp90 N-terminal domain and prime the chaperone activity. *J. Mol. Biol.* **415**, 3–15 (2012).
26. Lorenz, O. R. et al. Modulation of the Hsp90 chaperone cycle by a stringent client protein. *Mol. Cell* **53**, 941–953 (2014).
27. Street, T. O., Lavery, L. A. & Agard, D. A. Substrate binding drives large-scale conformational changes in the Hsp90 molecular chaperone. *Mol. Cell* **42**, 96–105 (2011).
28. Hessling, M., Richter, K. & Buchner, J. Dissection of the ATP-induced conformational cycle of the molecular chaperone Hsp90. *Nat. Struct. Mol. Biol.* **16**, 287–293 (2009).
29. Schubert, J., Schulze, A., Prodromou, C. & Neuweiler, H. Two-colour single-molecule photoinduced electron transfer fluorescence imaging microscopy of chaperone dynamics. *Nat. Commun.* **12**, 6964 (2021).
30. Saio, T., Guan, X., Rossi, P., Economou, A. & Kalodimos, C. G. Structural basis for protein antiaggregation activity of the trigger factor chaperone. *Science* **344**, 1250494 (2014).
31. Karagoz, G. E. et al. Hsp90-Tau complex reveals molecular basis for specificity in chaperone action. *Cell* **156**, 963–974 (2014).
32. Huang, C., Rossi, P., Saio, T. & Kalodimos, C. G. Structural basis for the antifolding activity of a molecular chaperone. *Nature* **537**, 202–206 (2016).
33. Huang, C. & Kalodimos, C. G. Structures of Large Protein Complexes Determined by Nuclear Magnetic Resonance Spectroscopy. *Annu Rev. Biophy.* **46**, 317–336 (2017).
34. Jiang, Y., Rossi, P. & Kalodimos, C. G. Structural basis for client recognition and activity of Hsp40 chaperones. *Science* **365**, 1313–1319 (2019).
35. Rosenzweig, R. & Kay, L. E. Bringing dynamic molecular machines into focus by methyl-TROSY NMR. *Annu. Rev. Biochem* **83**, 291–315 (2014).
36. Burmann, B. M. et al. Regulation of α-synuclein by chaperones in mammalian cells. *Nature* **577**, 127–132 (2020).
37. Faust, O. et al. HSP40 proteins use class-specific regulation to drive HSP70 functional diversity. *Nature* **587**, 489–494 (2020).
38. Qu, X. et al. Structural basis for the dynamic chaperoning of disordered clients by Hsp90. *Nat. Struct. Mol. Biol.* **31**, 1482–1491 (2024).
39. Sun, H., Kay, L. E. & Tugarinov, V. An optimized relaxation-based coherence transfer NMR experiment for the measurement of side-chain order in methyl-protonated, highly deuterated proteins. *J. Phys. Chem. B* **115**, 14878–14884 (2011).
40. Karagoz, G. E. et al. N-terminal domain of human Hsp90 triggers binding to the cochaperone p23. *Proc. Natl. Acad. Sci. USA* **108**, 580–585 (2011).

41. Pearl, L. H. Review: The HSP90 molecular chaperone-an enigmatic ATPase. *Biopolymers* **105**, 594–607 (2016).
42. Ratzke, C., Mickler, M., Hellenkamp, B., Buchner, J. & Hugel, T. Dynamics of heat shock protein 90 C-terminal dimerization is an important part of its conformational cycle. *Proc. Natl. Acad. Sci. USA* **107**, 16101–16106 (2010).
43. Korzhnev, D. M., Kloiber, K., Kanelis, V., Tugarinov, V. & Kay, L. E. Probing slow dynamics in high molecular weight proteins by methyl-TROSY NMR spectroscopy: application to a 723-residue enzyme. *J. Am. Chem. Soc.* **126**, 3964–3973 (2004).
44. Palmer, A. G. 3rd, Kroenke, C. D. & Loria, J. P. Nuclear magnetic resonance methods for quantifying microsecond-to-millisecond motions in biological macromolecules. *Methods Enzymol.* **339**, 204–238 (2001).
45. Morra, G., Potestio, R., Micheletti, C. & Colombo, G. Corresponding functional dynamics across the Hsp90 Chaperone family: insights from a multiscale analysis of MD simulations. *PLoS Comput. Biol.* **8**, e1002433 (2012).
46. Mader, S. L. et al. Conformational dynamics modulate the catalytic activity of the molecular chaperone Hsp90. *Nat. Commun.* **11**, 1410 (2020).
47. Cunningham, C. N., Southworth, D. R., Krukenberg, K. A. & Agard, D. A. The conserved arginine 380 of Hsp90 is not a catalytic residue, but stabilizes the closed conformation required for ATP hydrolysis. *Protein Sci.* **21**, 1162–1171 (2012).
48. Schmid, S., Gotz, M. & Hugel, T. Effects of Inhibitors on Hsp90's Conformational Dynamics, Cochaperone and Client Interactions. *Chemphyschem* **19**, 1716–1721 (2018).
49. Reidy, M., Garzillo, K. & Masison, D. C. Nucleotide exchange is sufficient for Hsp90 functions in vivo. *Nat. Commun.* **14**, 2489 (2023).
50. Park, S. J., Kostic, M. & Dyson, H. J. Dynamic Interaction of Hsp90 with Its Client Protein p53. *J. Mol. Biol.* **411**, 158–173 (2011).
51. Lee, B. L. et al. The Hsp90 Chaperone: (1)H and (19)F Dynamic Nuclear Magnetic Resonance Spectroscopy Reveals a Perfect Enzyme. *Biochemistry* **58**, 1869–1877 (2019).
52. Seifert, C. & Grater, F. Force distribution reveals signal transduction in E. coli Hsp90. *Biophys. J.* **103**, 2195–2202 (2012).
53. Blacklock, K. & Verkhivker, G. M. Computational modeling of allosteric regulation in the hsp90 chaperones: a statistical ensemble analysis of protein structure networks and allosteric communications. *PLoS Comput. Biol.* **10**, e1003679 (2014).
54. Henot, F. et al. Visualizing the transiently populated closed-state of human HSP90 ATP binding domain. *Nat. Commun.* **13**, 7601 (2022).
55. Kirschke, E., Goswami, D., Southworth, D., Griffin, P. R. & Agard, D. A. Glucocorticoid receptor function regulated by coordinated action of the Hsp90 and Hsp70 chaperone cycles. *Cell* **157**, 1685–1697 (2014).
56. Wand, A. J. & Sharp, K. A. Measuring Entropy in Molecular Recognition by Proteins. *Annu Rev. Biophys.* **47**, 41–61 (2018).
57. Delaglio, F. et al. NMRPipe: A multidimensional spectral processing system based on UNIX pipes. *J. Biomol. NMR* **6**, 277–293 (1995).
58. Sprangers, R. & Kay, L. E. Quantitative dynamics and binding studies of the 20S proteasome by NMR. *Nature* **445**, 618–622 (2007).
59. McDonald, L. R., Boyer, J. A. & Lee, A. L. Segmental Motions, Not a Two-State Concerted Switch, Underlie Allostery in CheY. *Structure* **20**, 1363–1373 (2012).
60. Bieri, M. & Gooley, P. R. Automated NMR relaxation dispersion data analysis using NESSY. *BMC Bioinforma.* **12**, 421 (2011).
61. Conicella, A. E. et al. An intrinsically disordered motif regulates the interaction between the p47 adaptor and the p97 AAA+ ATPase. *Proc. Natl Acad. Sci. USA* **117**, 26226–26236 (2020).
62. Chen, Y. et al. Assembly status transition offers an avenue for activity modulation of a supramolecular enzyme. *Elife* **10** (2021).

Acknowledgements

We gratefully acknowledge Dr. Y. Xia and Dr. T. Xie for insightful discussions and the BioNMR Laboratory of the Division of Life Sciences and Medicine at the University of Science and Technology of China for NMR data collection. A portion of this work was performed on the Steady High Magnetic Field Facilities, High Magnetic Field Laboratory, Chinese Academy of Sciences. This study was supported by the National Natural Science Foundation of China (32471273, 31971144, 31770807 and T2221005) to C.H., the National Key R&D Program of China (2024YFA1700123 and 2023YFC3403102) to C.H, and the Global Select Project DJK- LX-2022011 of the Institute of Health and Medicine, Hefei Comprehensive National Science Center to C.H.

Author contributions

C.H. and W.X. designed the research. X.Q., S.W., S. Z. and C. W. prepared the protein samples and conducted biochemical experiments. X.Q. and S.W. performed EM studies. X.Q. C. W. and C.H. performed the NMR experiments. C.H., X.Q., S.W., C.W., S.Z. and W.X. analyzed the data. C.H., X.Q. and W.X. drafted the manuscript. All authors reviewed and approved the final manuscript.

Competing interests

The authors declare no competing interests.

Additional information

Supplementary information The online version contains supplementary material available at https://doi.org/10.1038/s41467-024-55026-y.

Correspondence and requests for materials should be addressed to Weiya Xu or Chengdong Huang.

Peer review information *Nature Communications* thanks Anastasia Zhuravleva and the other, anonymous, reviewers for their contribution to the peer review of this work. A peer review file is available.